A method for identifying parameters of the conductivity coefficient of objects is generalized for the case of reconstructing an image of a part of a soil massif from the tomography data of the applied quasipotentials. In this case, without diminishing the generality, the reconstruction of the image is carried out in a fragment of a rectangular medium with local bursts of homogeneity present in it. The general idea of the corresponding algorithm consists in the sequential iterative solution of problems on quasiconformal mappings and identification of the parameters of the conductivity coefficient, with an insufficient amount of data on the values of the flow functions on the «inaccessible» part of the boundary. The image was reconstructed according to the data obtained using a full-range gradient array. The developed approach, in comparison with the existing ones, has a number of advantages that make it possible to increase the accuracy of identification of the conductivity coefficient. Namely, it provides an increase, in a qualitative sense, in the amount of input data, allows avoiding the use of Dirac delta functions when modeling areas of application of potentials and sufficiently flexibly take into account the mathematical aspects of the implementation of a quasiconformal mapping of a finite fragment of a half-plane onto a parametric polygon (domain of a complex quasipotential). The solution of the corresponding problem, in particular, occurs not in a single (fixed) investigated fragment of a rectangular soil massif, but in a number of smaller subdomains of the same shape, in the proposed optimal sequence. This saves machine time significantly. The prospects for further practical implementation of the proposed method follow from its ability to give an approximate result with relatively low costs (financial, time)

Keywords: electrical resistivity tomography, quasiconformal mappings, identification, inverse problems, numerical methods

UDC 519.6
DOI: 10.15587/1729-4061.2020.215045

GENERALIZATION OF NUMERICAL QUASICONFORMAL MAPPING METHODS FOR GEOLOGICAL PROBLEMS

A. Bomba
Doctor of Technical Sciences, Professor
Department of Computer Science and Applied Mathematics*
E-mail: a.ya.bomba@nuwm.edu.ua
M. Boichura
PhD
Research Department*
E-mail: m.v.boichura@nuwm.edu.ua
B. Sydorchuk
PhD, Associate Professor
Department of Automation, Electrical Engineering and Computer-Integrated Technologies*
E-mail: b.p.sydorchuk@nuwm.edu.ua
*National University of Water and Environmental Engineering
Soborna str., 11, Rivne, Ukraine, 33028

Received date 13.07.2020
Accepted date 16.10.2020
Published date 30.10.2020

1. Introduction

Modern approaches to identifying the structure of soil massifs differ in the level of convenience, complexity in use, price, and the like. Electrical resistivity tomography (ERT) methods have taken a significant place here, which, due to their conceptual simplicity, low cost of equipment and ease of use, are being applied in an increasing number of industries. This is the case in environmental research, hydrological research, mineral exploration, archaeological mapping, construction, and the like. For example, ERT is widely used to detect groundwater; this is especially important when solving the problem of landslides on hillsides. It is used in environmental studies when mapping abandoned industrial lands for metal or chemical waste residues. Also, the method is suitable for hydrological studies of zones under the bottom of rivers, lakes and even seas. It is used in the exploration of near-surface deposits of certain types of oil. It is used in engineering and geological studies for laying main pipelines under roads.

The main and significant disadvantage of ERT is the relatively low quality of the images obtained. This is due to both mathematical and technical aspects. First of all, due to the relatively high cost in time and the high cost of three-dimensional studies, the most appropriate are considered to be the corresponding two-dimensional applications. Moreover, to ensure the uniqueness of the solution, the number of specified boundary conditions must be very large and, in a sense, uniformly specified along the entire boundary. It is obvious that, especially in geological problems, it is generally impossible to comply with these conditions. Moreover, the averaging of electrical characteristics in the areas of potential application, which take place in traditional models, significantly negatively affects the resulting solution. The use of the Dirac delta function in such cases when modeling the contact area between the electrode and the investigated medium by a point leads to a certain mathematical inconsistency. Despite all the listed problems, on the one hand, and the economic feasibility of using ERT methods for identifying the soil structure, on the other, this study is relevant. This will allow to build more accurate maps of soil massifs.

2. Literature review and problem statement

In most cases of ERT application in the study of media structures, calculations are performed approximately. Namely:

by alternately solving subtasks for constructing current density fields and identifying parameters [1]. The latter is carried out using nonlinear methods, linear approximation methods, machine learning, backscattering, direct methods, etc. [1–3]. To construct the fields of current densities, in most cases, systems of equations of elliptic type are solved for given distributions of potentials and the corresponding derivatives along the normal along the entire boundary of the investigated body [1]. For this, finite-difference methods, the method of finite elements, finite volumes, etc. are usually used. [1–3]. In geological studies, information on the structure of the medium and its electrical characteristics is mainly limited to data from the surface [2]. Therefore, the issues of obtaining such measurements, which led to a qualitative result, are given considerable attention, especially taking into account the incorrectness of the original problem, in particular, according to Hadamard [1, 3]. In other words, there is instability, lack of unity or no denouement at all. In the process of iterative solution of the problem by means of EPT, when applying most of the methods, one usually has to deal with all three conditions of incorrectness. As a way out of this situation, a very laborious regularization procedure is used. In particular, the corresponding constants usually have to be selected experimentally. However, it should be noted that regularizations usually require only identification subproblems, which explicitly or implicitly contain matrix inversion procedures [3].

Taking into account, in particular, the problems with the input data, the important characteristics of the most common arrays (schemes) of charge injection and data collection are analyzed by examples and the corresponding comparisons are made. A number of characteristics are taken into account here, in particular, the value of the geometric factor. This value is the reciprocal of the potential difference. Obviously, the corresponding values are very large starting from the distance from the current electrodes. The sensitivity of the boundary conditions to the values of the conductivity coefficient (CC) at various points of the domain is determined using the Frechet derivative. The corresponding values tend to zero at large distances from the current electrodes. Sensitivity characterizes how much a change in the CC value at a particular point affects the measurements of the potential values on the surface. Signal-to-noise ratio characteristic is also analyzed.

Another important problem that arises when organizing the process of obtaining input data is the appropriate choice of array, depending on the characteristics of the environment under study. In [5], comparisons are made between the four-electrode gradient, dipole-dipole and Wenner arrays. Significant advantages of the gradient configuration over others in all parameters are noted. In [4], the values of the geometric factors of the dipole-dipole, gradient and Schlumberger arrays are compared. Here, the dipole-dipole configuration is defined as having the highest sensitivity to noise. Whereas the gradient is the smallest. This paper also proposes the use of a full-range gradient array, which also covers measurements outside the study area. This allows more data to be obtained, although it results in a slightly worse signal-to-noise ratio.

Moreover, there is a significantly different type of array. In works [2, 4] examples of the study of a soil massif between two wells, inside which electrodes are placed, are given. For such a case, in [4] it was proposed to use the following arrays: pole-pole, pole-bipole, bipole-pole and bipole-bipole. Also, in this work, a certain improvement of the finite element method is used to construct the current density fields – the Gaussian quadrature grid approach.

An important issue in the study of the structure of soil massifs is the presence of anisotropy effect. In [6], all existing problems, including regularization, are outlined in sufficient detail.

The work [2] describes the general idea of reconstruction of a three-dimensional image of a fragment of a soil massif. The specific results of the operation of the corresponding algorithms on real examples are also presented.

In general, when solving the problem of reconstructing the image of a soil massif by ERT means, it is assumed that the particles move according to Ohm's law $J=\sigma \mathrm{grad}\varphi$ where J is the current density, σ is the CC, and φ is the quasipotential. In most applications, the source of charges is considered «point», and when solving the corresponding problem, the current I is taken averaged over the volume of the contact V. Then, assuming $\mathrm{div}J=0$, the relationship between J and I is set in the form [2, 4]: $\mathrm{grad}(\sigma \mathrm{grad}\varphi)=-\delta(x-x_s)\delta(y-y_s)I/\Delta V$, where δ is the Dirac delta function, (x_s, y_s) is the coordinate of the current electrode.

Reconstruction of the image of the structure of a soil massif by ERT methods, in addition to the above, has a number of other mathematical and physical aspects [2]. First of all, it should be borne in mind that problems of this kind are solved in infinite domains using elliptic equations with known boundary conditions. Since in practice it is usually impossible to obtain such a volume of data, when reconstructing images, they are most often limited to the corresponding final fragment in the form of a rectangle [2, 4, 6] or a trapezoid [2, 4, 5, 7]. In general, to ensure maximum accuracy of calculations, the dimensions of these figures should be as large as possible. However, in order to speed up the calculations, the values of the corresponding parameters are selected depending on the array used, the availability of a priori data within the area and the values of the geometric factor. A separate problem is the implementation of quasiconformal mappings of a finite fragment of a half-plane [2, 8].

It should be noted that all of the above types of arrays have their own advantages and significant disadvantages, and are used depending on the structure of the studied environment and the corresponding boundary. However, in all cases there is an «acute» lack of data due to the difficulty of accessing deep soil layers. The use of Dirac delta functions in modeling the areas of application of potentials [2, 4, 7] distorts the resulting solution.

Thus, to date, the question of the «point nature» of the areas of application of potentials and the use of Dirac functions has not been resolved. The regularization problem is complex and ambiguous, which requires an experimental selection of constants. The problem of obtaining a large amount of data, also from the entire border of the domain, is unsolved. The boundaries of the studied environment, as a rule, are chosen very approximately. It is impossible to explore deep soil layers. There is no perfect array for collecting data from the border. The problem of time-consuming and high cost for obtaining a three-dimensional image has not been solved. Modern methods for solving subproblems of constructing current density fields and identifying parameters have their own advantages and disadvantages. In combination, the listed problems complement various inaccuracies and errors, which often lead to an unsatisfactory result. However, some of these issues, today, can be at least partially solved.

3. The aim and objectives of research

The aim of research is to extend the method of quasiconformal mappings in the case of identifying the CC parameters of a fragment of a soil massif with a known structure of the latter. This will allow obtaining more accurate images at relatively low costs in the field of environmental research, hydrological research, mineral exploration, archaeological mapping, construction, and the like.

To achieve this aim, the following objectives are formed:

– to modify the mathematical model of the tomography problem of the applied quasipotential in the body image reconstruction in the case of identifying the parameters of a fragment of a soil massif;

– to develop an algorithm for reconstructing the image of a part of a soil massif and write an appropriate computer program;

– to carry out numerical experiments and carry out their analysis.

4. Working hypothesis and formalization of the problem description

Without loss of generality, within the framework of this work, let's restrict ourselves to the use of a four-electrode full-range gradient array in the absence of simplification in terms of the «point-like» nature of the potential application areas. Such a data acquisition scheme, in comparison with others [2, 4], is characterized by a high density of input data, relatively low sensitivity to «noise» and relatively small values of the geometric factor. Therefore, this array, in most cases, allows to obtain the most accurate results precisely in the near-surface zones.

As noted above, in ERT there is an «acute» problem of lack of input data, the use of Dirac functions in modeling the areas of application of potentials and the complexity of the implementation of quasiconformal mappings of a finite fragment of a half-plane. To increase in a qualitative sense the number of the first, to avoid the second and at the same time to flexibly take into account the third possible based on research [8–10]. In particular, they dealt with precisely these problems, but in environments with discretely specified boundary conditions along the entire boundary. Namely, in [8], the issues of flow formation in the presence of several sections of application of quasipotentials were studied in detail. In [9, 10], a new technique (method and corresponding algorithms) was developed for the complex analysis of solving tomography problems of applied quasipotentials. It provides, for each of the corresponding injection, the presence on the boundary of the domain of only equipotential lines, with given functions of local current densities, and streamlines, with known distributions of the quasipotential on them. In [9], the technique is concretized in the case of media with available local bursts of homogeneous materials. Here CC is sought in the form:

$$\sigma\left(x,y,\chi,\alpha_1,\varepsilon_1,x_1,y_1,...,\alpha_s,\varepsilon_s,x_s,y_s\right)= \\ =\chi+\sum_{k=1}^{s}\frac{\alpha_k}{1+\left(\left(x-x_k\right)^2+\left(y-y_k\right)^2\right)/\varepsilon_k}, \qquad (1)$$

where χ, α_k, ε_k, x_k, y_k ($k=1, ..., s$) are parameters determined in the process of solving the problem, s is the number of bursts.

Without loss of generality, in this work, the infinite half-plane (soil massif) will be replaced by a rectangular domain (a fragment of the vertical section of the soil massif) G_z (Fig. 1, *a*). The corresponding limits are set by four line segments B^0B^1: $x=-a/2$, $0\le y\le b$; $B^1B_pA_pD_pC_pC^0$: $y=0$, $-a/2\le x\le a/2$; C^0C^1: $x=a/2$, $0\le y\le b$; B^1C^1: $y=b$, $-a/2\le x\le a/2$. On a part of the boundary (on some equipotential lines) set quasipotentials:

$$\varphi^{(p)}\Big|_{A_pB_p}=\varphi_*^{(p)},\ \ \varphi^{(p)}\Big|_{B^0B^1C^1C^0}=\varphi_0^{(p)},$$

$$\varphi^{(p)}\Big|_{C_pD_p}=\varphi^{*(p)},\ \ \left(\varphi_*^{(p)}<\varphi_0^{(p)}<\varphi^{*(p)}\right), \qquad (2)$$

obtained in the process of transmission of electric charges and simultaneous measurements, where $p=1,2,...$ is the injection number [9, 10]; $\varphi^{(p)}=\varphi^{(p)}(x,y)$ are quasipotentials; A_p, O_{*p}, B_p, B^0, B^1, $\bar{O}_p$, C^1, C^0, C_p, O_p^*, D_p, $\bar{O}_p$ are marked points on ∂G_z; a and b – longitudinal and transverse dimensions of the investigated domain (rectangle); B^0B_p, C^0C_p and A_pD_p are impenetrable boundary lines of currents. Current injection through the tomographic cross section, similarly to [9, 10], is modeled by points

$$\left(x_A^{(p)},y_A^{(p)}\right),\left(x_{O_*}^{(p)},y_{O_*}^{(p)}\right),\left(x_B^{(p)},y_B^{(p)}\right),$$

$$\left(x_{B^0},y_{B^0}\right)=\left(-a/2,0\right),\left(x_{B^1},y_{B^1}\right)=\left(-a/2,b\right),\left(x_{\bar{O}}^{(p)},y_{\bar{O}}^{(p)}\right),$$

$$\left(x_{C^1},y_{C^1}\right)=\left(a/2,b\right),\ \left(x_{C^0},y_{C^0}\right)=\left(a/2,0\right),\ \left(x_C^{(p)},y_C^{(p)}\right),$$

$$\left(x_{O^*}^{(p)},y_{O^*}^{(p)}\right),\left(x_D^{(p)},y_D^{(p)}\right),\left(x_{\underline{O}}^{(p)},y_{\underline{O}}^{(p)}\right),$$

according to which

$$A_p=\left(x_A^{(p)},y_A^{(p)}\right),\ O_{*p}=\left(x_{O_*}^{(p)},y_{O_*}^{(p)}\right),\ B_p=\left(x_B^{(p)},y_B^{(p)}\right),$$

$$B^0=\left(x_{B^0},y_{B^0}\right),\ B^1=\left(x_{B^1},y_{B^1}\right),\ \bar{O}_p=\left(x_{\bar{O}}^{(p)},y_{\bar{O}}^{(p)}\right),$$

$$C^1=\left(x_{C^1},y_{C^1}\right),\ C^0=\left(x_{C^0},y_{C^0}\right),\ C_p=\left(x_C^{(p)},y_C^{(p)}\right),$$

$$O_p^*=\left(x_{O^*}^{(p)},y_{O^*}^{(p)}\right),\ D_p=\left(x_D^{(p)},y_D^{(p)}\right),\ \underline{O}_p=\left(x_{\underline{O}}^{(p)},y_{\underline{O}}^{(p)}\right).$$

The corresponding to the given injection boundary of the domain G_z with the given four marked points on it is denoted by $\partial G_z^{(p)}$ ($z^{(p)}=x^{(p)}+iy^{(p)}$).

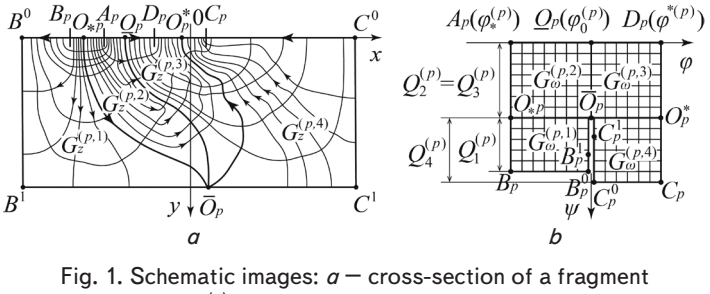

Fig. 1. Schematic images: *a* – cross-section of a fragment of a soil massif $G_z^{(p)}$; *b* – corresponding domains of the complex quasipotential $G_\omega^{(p)}$

The solution of geological problems by ERT means, in most cases [2, 4, 7], occurs with the use of Dirac delta functions in the areas of application of quasipotentials.

In this work, the corresponding formulation, provided that the parameters of the CC $\sigma=\sigma(x,y)$ are identified and the quasipotentials $\varphi^{(p)}=\varphi^{(p)}(x,y)$ are found in the form (1), (2),

$$\frac{\partial}{\partial x}\left(\sigma\frac{\partial\varphi^{(p)}}{\partial x}\right)+\frac{\partial}{\partial y}\left(\sigma\frac{\partial\varphi^{(p)}}{\partial y}\right)=0; \quad (3)$$

$$\left.\frac{\partial\varphi^{(p)}(M)}{\partial n}\right|_{B^0B_p\cup A_pD_p\cup C^0C_p}=0; \quad (4)$$

$$\varphi^{(p)}(M)\big|_{B^0B_p}=\overline{\varphi}^{(p)}(M),\ \varphi^{(p)}(M)\big|_{A_pD_p}=\underline{\varphi}^{(p)}(M),$$

$$\varphi^{(p)}(M)\big|_{C^0C_p}=\overline{\overline{\varphi}}^{(p)}(M); \quad (5)$$

$$\sigma\left.\frac{\partial\varphi^{(p)}(M)}{\partial n}\right|_{A_pB_p}=\Psi_*^{(p)}(M),$$

$$\sigma\left.\frac{\partial\varphi^{(p)}(M)}{\partial n}\right|_{C_pD_p}=\Psi^{*(p)}(M), \quad (6)$$

where M is the current point of the corresponding curve; n is the unit outward normal vector. Functions

$$\overline{\varphi}^{(p)}(M)=\overline{\varphi}^{(p)}(x,...)\ \left(x_{B^0}^{(p)}\le x\le x_B^{(p)}\right),$$

$$\overline{\overline{\varphi}}^{(p)}(M)=\overline{\overline{\varphi}}^{(p)}(x,...)\ \left(x_C^{(p)}\le x\le x_{C^0}^{(p)}\right),$$

$$\underline{\varphi}^{(p)}(M)=\underline{\varphi}^{(p)}(x,...)\ \left(x_A^{(p)}\le x\le x_D^{(p)}\right),$$

$$\Psi_*^{(p)}(M)=\Psi_*^{(p)}(x,...)\ \left(x_B^{(p)}\le x\le x_A^{(p)}\right),$$

$$\Psi^{*(p)}(M)=\Psi^{*(p)}(x,...)\ \left(x_D^{(p)}\le x\le x_C^{(p)}\right),$$

similar to [9, 10] can be constructed by interpolating their experimentally obtained values

$$\overline{\varphi}_{\overline{i}^{(p)}}^{(p)},\ \overline{\overline{\varphi}}_{\overline{\overline{i}}^{(p)}}^{(p)},\ \underline{\varphi}_{\underline{i}^{(p)}}^{(p)},\ \Psi_{*j_*^{(p)}}^{(p)},\ \Psi_{j^{*(p)}}^{*(p)}$$

for some

$$x=\overline{x}_{\overline{i}^{(p)}}^{(p)},\ x=\overline{\overline{x}}_{\overline{\overline{i}}^{(p)}}^{(p)},\ x=\underline{x}_{\underline{i}^{(p)}}^{(p)},\ x=x_{*j_*^{(p)}}^{(p)},\ x=x_{j^{*(p)}}^{*(p)}$$

in the sections B^0B_p, C^0C_p, A_pD_p, A_pB_p, C_pD_p, respectively:

$$\varphi_*^{(p)}\le\underline{\varphi}_{\underline{i}^{(p)}}^{(p)}\le\varphi^{*(p)},\ \varphi_*^{(p)}\le\overline{\varphi}_{\overline{i}^{(p)}}^{(p)}\le\varphi_0^{(p)},\ \varphi_0^{(p)}\le\overline{\overline{\varphi}}_{\overline{\overline{i}}^{(p)}}^{(p)}\le\varphi^{*(p)},$$

$$\Psi_{*j_*^{(p)}}^{(p)}>0,\ \Psi_{j^{*(p)}}^{*(p)}>0,\ \overline{i}^{(p)}=\overline{0,\overline{m}^{(p)}+1},\ \overline{\overline{i}}^{(p)}=\overline{0,\overline{\overline{m}}^{(p)}+1},$$

$$\underline{i}^{(p)}=\overline{0,\underline{m}^{(p)}+1},\ j_*^{(p)}=\overline{0,n_*^{(p)}+1},\ j^{*(p)}=\overline{0,n^{*(p)}+1}.$$

Let's note that in most practical cases of identification of the soil structure by ERT means, there is no possibility to obtain (measure) the values of functions

$$\sigma\frac{\partial\varphi^{(p)}(M)}{\partial n}$$

in sections of the $B^0B^1C^1C^0$ type. Therefore, the corresponding problems, in particular (1)–(6), have, generally speaking, an infinite number of solutions. However, it should be noted that they differ little from each other in the subdomain with a sufficiently large value of the geometric factor; usually these are near-surface soil layers [2, 4].

5. Materials and methods of research (modification of problem (1)–(6) and its difference analogue)

A typical approach to solving problems (1)–(6) involves the averaging of functions (6) and the introduction of the Dirac delta into differential equations (3) [2, 4, 7]. To avoid such a rather «rough» simplification, let's propose, like [8–10], to introduce quasiharmonic functions $\psi^{(p)}(x,y)$ (flow functions), complex conjugate to $\varphi^{(p)}(x,y)$ and replace (3), (4) and (6) on

$$\sigma\frac{\partial\varphi^{(p)}}{\partial x}=\frac{\partial\psi^{(p)}}{\partial y},\ \sigma\frac{\partial\varphi^{(p)}}{\partial y}=-\frac{\partial\psi^{(p)}}{\partial x}; \quad (7)$$

$$\psi^{(p)}\big|_{A_pD_p}=0,\ \psi^{(p)}\big|_{B^0B_p}=Q_1^{(p)}+Q_2^{(p)},$$

$$\psi^{(p)}\big|_{C^0C_p}=Q_3^{(p)}+Q_4^{(p)}; \quad (8)$$

$$\psi^{(p)}(M)\big|_{A_pB_p}=\psi_*^{(p)}(M),\ \psi^{(p)}(M)\big|_{C_pD_p}=\psi^{*(p)}(M). \quad (9)$$

Thus, from problem (1)–(6) let's pass to its generalized analogue (2), (5), (7)–(9) onto quasiconformal mappings $\omega=\omega^{(p)}(z)=\varphi^{(p)}(x,y)+i\psi^{(p)}(x,y)$ of physical domains

$$G_z^{(p)}=\bigcup_{\xi=1}^4 G_z^{(p,\xi)}\cup\bigcup_{\xi=1}^3 G_z^{(p,\xi)}\cap G_z^{(p,\xi+1)}\ \text{(Fig. 1, } a\text{)}$$

to the corresponding domains of the complex quasipotential

$$G_\omega^{(p)}=\bigcup_{\xi=1}^4 G_\omega^{(p,\xi)}\cup\bigcup_{\xi=1}^3 G_\omega^{(p,\xi)}\cap G_\omega^{(p,\xi+1)}\ \text{(Fig. 1, } b\text{)}$$

subject to CC identification (1) [8, 10], where dl is the arc element of the corresponding curve; $\varphi_0^{(p)}=\varphi|_{\overline{O}_p}$; $Q_1^{(p)}+Q_2^{(p)}$ and $Q_4^{(p)}$ are the discharges entering the domain $G_z^{(p)}$ through the sections A_pB_p and $\overline{O}_pC^0$, respectively; $Q_3^{(p)}+Q_4^{(p)}$ and $Q_1^{(p)}$ are the discharges leaving it through the sections C_pD_p and $\overline{O}_pB^0$, respectively;

$$\int_{A_pB_p}\sigma\varphi_n'^{(p)}(M)\,dl=Q_1^{(p)}+Q_2^{(p)},$$

$$\psi_*^{(p)}(M)=\int_{A_pM}\Psi_*^{(p)}(M)\,dl,$$

$$\int_{\overline{O}_pB^0}\sigma\varphi_n'^{(p)}(M)\,dl=Q_1^{(p)},$$

$$\int_{\overline{O}_pC^0}\sigma\varphi_n'^{(p)}(M)\,dl=Q_4^{(p)},$$

$$\psi^{*(p)}(M)=\int_{D_pM}\Psi^{*(p)}(M)\,dl,$$

$$\int_{D_pC_p}\sigma\varphi_n'^{(p)}(M)\,dl=Q_3^{(p)}+Q_4^{(p)};$$

$$G_\omega^{(p,1)}=\left\{\begin{matrix}\omega^{(p)}:\varphi_*^{(p)}<\varphi^{(p)}<\varphi_0^{(p)},\\ Q_2^{(p)}<\psi^{(p)}<Q_1^{(p)}+Q_2^{(p)}\end{matrix}\right\},$$

$$G_\omega^{(p,2)}=\left\{\omega^{(p)}:\varphi_*^{(p)}<\varphi^{(p)}<\varphi_0^{(p)},0<\psi^{(p)}<Q_2^{(p)}\right\},$$

$$G_\omega^{(p,3)}=\left\{\begin{matrix}\omega^{(p)}:\varphi_0^{(p)}<\varphi^{(p)}<\varphi^{*(p)},\\ 0<\psi^{(p)}<Q_3^{(p)}\end{matrix}\right\},$$

$$G_\omega^{(p,4)}=\left\{\begin{matrix}\omega^{(p)}:\varphi_0^{(p)}<\varphi^{(p)}<\varphi^{*(p)},\\ Q_3^{(p)}<\psi^{(p)}<Q_3^{(p)}+Q_4^{(p)}\end{matrix}\right\}.$$

Taking into account the unconditional advantages [8] of passing to back reflections $z^{(p)}(\omega)=x^{(p)}(\varphi,\psi)+iy^{(p)}(\varphi,\psi)$ of

domains $G_{\omega}^{(p)}$ on domains $G_{z}^{(p)}$, let's write problem (1), (2) (5), (7)–(9) in the form [8, 10]:

$$\frac{\partial x^{(p)}}{\partial\varphi}=\sigma\frac{\partial y^{(p)}}{\partial\psi},\quad \frac{\partial y^{(p)}}{\partial\varphi}=-\sigma\frac{\partial x^{(p)}}{\partial\psi}; \tag{10}$$

$$x^{(p)}\left(\varphi,Q_2^{(p)}-0\right)=x^{(p)}\left(\varphi,Q_2^{(p)}+0\right),$$

$$y^{(p)}\left(\varphi,Q_2^{(p)}-0\right)=y^{(p)}\left(\varphi,Q_2^{(p)}+0\right),$$

$$\left(\varphi_*^{(p)}\le\varphi<\varphi_0^{(p)}\cup\varphi_0^{(p)}<\varphi\le\varphi^{*(p)}\right),$$

$$x^{(p)}\left(\varphi_0^{(p)}-0,\psi\right)=x^{(p)}\left(\varphi_0^{(p)}+0,\psi\right),$$

$$y^{(p)}\left(\varphi_0^{(p)}-0,\psi\right)=y^{(p)}\left(\varphi_0^{(p)}+0,\psi\right),\ \left(0\le\psi\le Q_2^{(p)}\right); \tag{11}$$

$$x^{(p)}\left(\varphi,Q_1^{(p)}+Q_2^{(p)}\right)=\overline{x}^{(p)}(\varphi),$$

$$y^{(p)}\left(\varphi,Q_1^{(p)}+Q_2^{(p)}\right)=0\ \left(\varphi_*^{(p)}\le\varphi\le\varphi_0^{(p)}\right),$$

$$x^{(p)}(\varphi,0)=\underline{x}^{(p)}(\varphi),\quad y^{(p)}(\varphi,0)=0\ \left(\varphi_*^{(p)}\le\varphi\le\varphi^{*(p)}\right),$$

$$x^{(p)}\left(\varphi,Q_3^{(p)}+Q_4^{(p)}\right)=\overline{\overline{x}}^{(p)}(\varphi),$$

$$y^{(p)}\left(\varphi,Q_3^{(p)}+Q_4^{(p)}\right)=0\ \left(\varphi_0^{(p)}\le\varphi\le\varphi^{*(p)}\right),$$

$$x^{(p)}\left(\varphi_*^{(p)},\psi\right)=x_*^{(p)}(\psi),$$

$$y^{(p)}\left(\varphi_*^{(p)},\psi\right)=0\ \left(0\le\psi\le Q_1^{(p)}+Q_2^{(p)}\right),$$

$$x^{(p)}\left(\varphi^{*(p)},\psi\right)=x^{*(p)}(\psi),$$

$$y^{(p)}\left(\varphi^{*(p)},\psi\right)=0\ \left(0\le\psi\le Q_3^{(p)}+Q_4^{(p)}\right),$$

$$-a/2\le x^{(p)}\left(\varphi_0^{(p)}-0,\psi\right)\le x_{\underline{Q}}^{(p)},$$

$$y^{(p)}\left(\varphi_0^{(p)}-0,\psi\right)=b\ \left(0\le\psi-Q_2^{(p)}\le Q_{B^1}^{(p)}\right),$$

$$x^{(p)}\left(\varphi_0^{(p)}-0,\psi\right)=-a/2,$$

$$0\le y^{(p)}\left(\varphi_0^{(p)}-0,\psi\right)\le b\ \left(Q_{B^1}^{(p)}<\psi-Q_2^{(p)}\le Q_1^{(p)}\right),$$

$$x_{\underline{Q}}^{(p)}\le x^{(p)}\left(\varphi_0^{(p)}+0,\psi\right)\le a/2,$$

$$y^{(p)}\left(\varphi_0^{(p)}+0,\psi\right)=b\ \left(0\le\psi-Q_3^{(p)}\le Q_{C^1}^{(p)}\right),$$

$$x^{(p)}\left(\varphi_0^{(p)}+0,\psi\right)=a/2,$$

$$0\le y^{(p)}\left(\varphi_0^{(p)}+0,\psi\right)\le b\ \left(Q_{C^1}^{(p)}<\psi-Q_3^{(p)}\le Q_4^{(p)}\right) \tag{12}$$

subject to identification (1), where $x=\overline{x}^{(p)}(\varphi)$, $x=\underline{x}^{(p)}(\varphi)$, $x=\overline{\overline{x}}^{(p)}(\varphi)$, $x=x_*^{(p)}(\psi)$, $x=x^{*(p)}(\psi)$ are the functions constructed by interpolating their experimentally obtained values $\overline{x}_{\overline{i}}^{(p)}$, $\underline{x}_{\underline{i}}^{(p)}$, $\overline{\overline{x}}_{\overline{\overline{i}}}^{(p)}$, $x_{*j_*}^{(p)}$, $x_{j^*}^{*(p)}$ for some arguments $\overline{\varphi}_{\overline{i}}^{(p)}$, $\underline{\varphi}_{\underline{i}}^{(p)}$, $\overline{\overline{\varphi}}_{\overline{\overline{i}}}^{(p)}$, $\psi_{*j_*}^{(p)}$, $\psi_{j^*}^{*(p)}$ on the segments B^0B_p, A_pD_p, C^0C_p, A_pB_p and C_pD_p, respectively; $Q_2^{(p)}+Q_{B^1}^{(p)}$ and $Q_3^{(p)}+Q_{C^1}^{(p)}$ are the values of discharges at points B^1 and C^1, respectively. Moreover, for an approximate solution of this problem, instead of generalizations of the Cauchy-Riemann conditions (10), it is convenient to use generalizations of the Laplace equations at all interior points of the domains $G_{\omega}^{(p)}$ and the orthogonality conditions on their boundaries [8]:

$$\begin{cases}\dfrac{\partial}{\partial\varphi}\left(\dfrac{1}{\sigma}\dfrac{\partial x^{(p)}}{\partial\varphi}\right)+\dfrac{\partial}{\partial\psi}\left(\sigma\dfrac{\partial x^{(p)}}{\partial\psi}\right)=0,\\ \dfrac{\partial}{\partial\varphi}\left(\dfrac{1}{\sigma}\dfrac{\partial y^{(p)}}{\partial\varphi}\right)+\dfrac{\partial}{\partial\psi}\left(\sigma\dfrac{\partial y^{(p)}}{\partial\psi}\right)=0;\end{cases} \tag{13}$$

$$\begin{cases}\dfrac{\partial x^{(p)}\left(\varphi,Q_1^{(p)}+Q_2^{(p)}\right)}{\partial\psi}=0,\ \varphi\in\left(\varphi_*^{(p)},\varphi_0^{(p)}\right),\\ \dfrac{\partial x^{(p)}(\varphi,0)}{\partial\psi}=0,\ \varphi\in\left(\varphi_*^{(p)},\varphi^{*(p)}\right),\\ \dfrac{\partial x^{(p)}\left(\varphi,Q_3^{(p)}+Q_4^{(p)}\right)}{\partial\psi}=0,\ \varphi\in\left(\varphi_0^{(p)},\varphi^{*(p)}\right),\\ \dfrac{\partial x^{(p)}\left(\varphi_0^{(p)},Q_2^{(p)}\right)}{\partial\psi}=0,\\ \dfrac{\partial x^{(p)}\left(\varphi_*^{(p)},\psi\right)}{\partial\varphi}=0,\ \psi\in\left(0,Q_1^{(p)}+Q_2^{(p)}\right),\\ \dfrac{\partial x^{(p)}\left(\varphi^{*(p)},\psi\right)}{\partial\varphi}=0,\ \psi\in\left(0,Q_3^{(p)}+Q_4^{(p)}\right),\\ \dfrac{\partial x^{(p)}\left(\varphi_0^{(p)}-0,\psi\right)}{\partial\varphi}=0,\ \psi\in\left(Q_2^{(p)},Q_2^{(p)}+Q_{B^1}^{(p)}\right],\\ \dfrac{\partial y^{(p)}\left(\varphi_0^{(p)}-0,\psi\right)}{\partial\varphi}=0,\ \psi\in\left[Q_2^{(p)}+Q_{B^1}^{(p)},Q_1^{(p)}+Q_2^{(p)}\right),\\ \dfrac{\partial x^{(p)}\left(\varphi_0^{(p)}+0,\psi\right)}{\partial\varphi}=0,\ \psi\in\left(Q_3^{(p)},Q_3^{(p)}+Q_{C^1}^{(p)}\right],\\ \dfrac{\partial y^{(p)}\left(\varphi_0^{(p)}+0,\psi\right)}{\partial\varphi}=0,\ \psi\in\left[Q_3^{(p)}+Q_{C^1}^{(p)},Q_3^{(p)}+Q_4^{(p)}\right).\end{cases} \tag{14}$$

Let's carry out the CC reconstruction with minimization of the functional [10], which does not provide for the use of matrix inversion procedures, and therefore does not require regularization [3]:

$$\Phi(\sigma)=$$

$$=\sum_{p=1}^{\tilde{p}}\sum_{(\tilde{x}_{i,j}^{(p)},\tilde{y}_{i,j}^{(p)})\in\overline{G}_z^{(p)}}\left(\sigma\begin{pmatrix}\tilde{x}_{i,j}^{(p)},\tilde{y}_{i,j}^{(p)},\chi,\alpha_1,\varepsilon_1,x_1,\\ y_1,\ldots,\alpha_s,\varepsilon_s,x_s,y_s\end{pmatrix}-f\left(\tilde{x}_{i,j}^{(p)},\tilde{y}_{i,j}^{(p)}\right)\right)^2\to\min. \tag{15}$$

Here, the summation is carried out over the data at the running nodes $\left(\tilde{x}_{i,j}^{(p)},\tilde{y}_{i,j}^{(p)}\right)$ of the corresponding dynamic grid, and only at points with a sufficiently large value of the geometric factor;

$$f\left(x^{(p)},y^{(p)}\right)=\sqrt{\left(\frac{\partial x^{(p)}}{\partial\varphi}\right)^2+\left(\frac{\partial y^{(p)}}{\partial\varphi}\right)^2}\Big/\sqrt{\left(\frac{\partial x^{(p)}}{\partial\psi}\right)^2+\left(\frac{\partial y^{(p)}}{\partial\psi}\right)^2}$$

is a function that characterizes a certain «iterative-intermediate» CC distribution at the p-th injection.

An approximate solution of problem (1), (11)–(14) under the condition of minimization of functional (15) is sought, similarly to [8, 10], on a uniform grid in network domains

$$G_{\omega}^{\gamma(p)}=\bigcup_{\xi=1}^{4}G_{\omega}^{\gamma(p,\xi)}\cup\bigcup_{\xi=1}^{3}G_{\omega}^{\gamma(p,\xi)}\cap G_{\omega}^{\gamma(p,\xi+1)},$$

where

$$G_{\omega}^{\gamma(p,1)}=\begin{cases}\left(\varphi_i^{(p,1)},\psi_j^{(p,1)}\right):\varphi_i^{(p,1)}=\varphi_*^{(p)}+i\Delta\varphi^{(p,1)},i=\overline{0,m_1^{(p)}};\\ \psi_j^{(p,1)}=Q_2^{(p)}+j\Delta\psi^{(p,1)},j=\overline{0,n_1^{(p)}};\\ \Delta\varphi^{(p,1)}=\left(\varphi_0^{(p)}-\varphi_*^{(p)}\right)/m_1^{(p)},\\ \Delta\psi^{(p,1)}=Q_1^{(p)}/n_1^{(p)},\gamma^{(p,1)}=\Delta\varphi^{(p,1)}/\Delta\psi^{(p,1)}\end{cases},$$

$$G_{\omega}^{\gamma(p,2)}=\left\{\begin{array}{l}\left(\varphi_i^{(p,2)},\psi_j^{(p,2)}\right):\varphi_i^{(p,2)}=\varphi_*^{(p)}+i\Delta\varphi^{(p,2)},\\ i=\overline{0,m_2^{(p)}};\psi_j^{(p,2)}=j\Delta\psi^{(p,2)},j=\overline{0,n_2^{(p)}};\\ \Delta\varphi^{(p,2)}=\left(\varphi_0^{(p)}-\varphi_*^{(p)}\right)/m_2^{(p)},\\ \Delta\psi^{(p,2)}=Q_2^{(p)}/n_2^{(p)},\gamma^{(p,2)}=\Delta\varphi^{(p,2)}/\Delta\psi^{(p,2)}\end{array}\right\},$$

$$G_{\omega}^{\gamma(p,3)}=\left\{\begin{array}{l}\left(\varphi_i^{(p,3)},\psi_j^{(p,3)}\right):\varphi_i^{(p,3)}=\varphi_*^{(p)}+\varphi_0^{(p)}+i\Delta\varphi^{(p,3)},\\ i=\overline{0,m_3^{(p)}};\psi_j^{(p,3)}=j\Delta\psi^{(p,3)},j=\overline{0,n_3^{(p)}};\\ \Delta\varphi^{(p,3)}=\left(\varphi^{*(p)}-\varphi_0^{(p)}\right)/m_3^{(p)},\\ \Delta\psi^{(p,3)}=Q_3^{(p)}/n_3^{(p)},\gamma^{(p,3)}=\Delta\varphi^{(p,3)}/\Delta\psi^{(p,3)}\end{array}\right\},$$

$$G_{\omega}^{\gamma(p,4)}=\left\{\begin{array}{l}\left(\varphi_i^{(p,4)},\psi_j^{(p,4)}\right):\varphi_i^{(p,4)}=\varphi_*^{(p)}+\varphi_0^{(p)}+i\Delta\varphi^{(p,4)},\\ i=\overline{0,m_4^{(p)}};\psi_j^{(p,4)}=Q_3^{(p)}+j\Delta\psi^{(p,4)},j=\overline{0,n_4^{(p)}};\\ \Delta\varphi^{(p,4)}=\left(\varphi^{*(p)}-\varphi_0^{(p)}\right)/m_4^{(p)},\\ \Delta\psi^{(p,4)}=Q_4^{(p)}/n_4^{(p)},\gamma^{(p,4)}=\Delta\varphi^{(p,4)}/\Delta\psi^{(p,4)}\end{array}\right\}.$$

In this case, let's write the corresponding difference representations in the form [8, 10]:

$$\left\{\begin{array}{l}x_{i,j}^{(p,\xi)}=\dfrac{0.5}{1+\tilde{\gamma}^{(p,\xi)2}\sigma_{i,j}^{\gamma(p,\xi)2}}\times\\ \times\left(\begin{array}{l}x_{i+1,j}^{(p,\xi)}+x_{i-1,j}^{(p,\xi)}+\tilde{\gamma}^{(p,\xi)2}\sigma_{i,j}^{\gamma(p,\xi)2}\times\\ \times\left(x_{i,j-1}^{(p,\xi)}+x_{i,j+1}^{(p,\xi)}\right)+\left(\begin{array}{l}\dfrac{\partial\sigma_{i,j}^{\gamma(p,\xi)}}{\partial x}\left(x_{i,j+1}^{(p,\xi)}-x_{i,j-1}^{(p,\xi)}\right)+\\ +\dfrac{\partial\sigma_{i,j}^{\gamma(p,\xi)}}{\partial y}\left(y_{i,j+1}^{(p,\xi)}-y_{i,j-1}^{(p,\xi)}\right)\end{array}\right)\times\\ \times\dfrac{0.25\tilde{\gamma}^{(p,\xi)2}\sigma_{i,j}^{\gamma(p,\xi)}}{\left(x_{i,j+1}^{(p,\xi)}-x_{i,j-1}^{(p,\xi)}\right)^{-1}}-\\ -\left(\begin{array}{l}\dfrac{\partial\sigma_{i,j}^{\gamma(p,\xi)}}{\partial x}\left(x_{i+1,j}^{(p,\xi)}-x_{i-1,j}^{(p,\xi)}\right)+\\ +\dfrac{\partial\sigma_{i,j}^{\gamma(p,\xi)}}{\partial y}\left(y_{i+1,j}^{(p,\xi)}-y_{i-1,j}^{(p,\xi)}\right)\end{array}\right)\dfrac{x_{i+1,j}^{(p,\xi)}-x_{i-1,j}^{(p,\xi)}}{4\sigma_{i,j}^{\gamma(p,\xi)}}\end{array}\right),\\ y_{i,j}^{(p,J)}=\dfrac{0.5}{1+\tilde{\gamma}^{(p,\xi)2}\sigma_{i,j}^{\gamma(p,\xi)2}}\times\\ \times\left(\begin{array}{l}y_{i+1,j}^{(p,\xi)}+y_{i-1,j}^{(p,\xi)}+\tilde{\gamma}^{(p,\xi)2}\sigma_{i,j}^{\gamma(p,\xi)2}\times\\ \times\left(y_{i,j-1}^{(p,\xi)}+y_{i,j+1}^{(p,\xi)}\right)+\left(\begin{array}{l}\dfrac{\partial\sigma_{i,j}^{\gamma(p,\xi)}}{\partial x}\left(x_{i,j+1}^{(p,\xi)}-x_{i,j-1}^{(p,\xi)}\right)+\\ +\dfrac{\partial\sigma_{i,j}^{\gamma(p,\xi)}}{\partial y}\left(y_{i,j+1}^{(p,\xi)}-y_{i,j-1}^{(p,\xi)}\right)\end{array}\right)\times\\ \times\dfrac{0.25\tilde{\gamma}^{(p,\xi)2}\sigma_{i,j}^{\gamma(p,\xi)}}{\left(y_{i,j+1}^{(p,\xi)}-y_{i,j-1}^{(p,\xi)}\right)^{-1}}-\\ -\left(\begin{array}{l}\dfrac{\partial\sigma_{i,j}^{\gamma(p,\xi)}}{\partial x}\left(x_{i+1,j}^{(p,\xi)}-x_{i-1,j}^{(p,\xi)}\right)+\\ +\dfrac{\partial\sigma_{i,j}^{\gamma(p,\xi)}}{\partial y}\left(y_{i+1,j}^{(p,\xi)}-y_{i-1,j}^{(p,\xi)}\right)\end{array}\right)\dfrac{y_{i+1,j}^{(p,\xi)}-y_{i-1,j}^{(p,\xi)}}{4\sigma_{i,j}^{\gamma(p,\xi)}}\end{array}\right);\end{array}\right. \quad (16)$$

$$x_{i,n_1^{(p)}}^{(p,1)}=\bar{x}^{(p)}\left(\varphi_i^{(p,1)}\right),\ \ y_{i,n_1^{(p)}}^{(p,1)}=0\ \left(0\le i\le m_1^{(p)}\right),$$

$$x_{i,0}^{(p,2)}=\underline{x}^{(p)}\left(\varphi_i^{(p,2)}\right),\ \ y_{i,0}^{(p,2)}=0\ \left(0\le i\le m_2^{(p)}\right),$$

$$x_{i,0}^{(p,3)}=\underline{x}^{(p)}\left(\varphi_i^{(p,3)}\right),\ \ y_{i,0}^{(p,3)}=0\ \left(0\le i\le m_3^{(p)}\right),$$

$$x_{i,n_4^{(p)}}^{(p,4)}=\bar{\bar{x}}^{(p)}\left(\varphi_i^{(p,4)}\right),\ \ y_{i,n_4^{(p)}}^{(p,4)}=0\ \left(0\le i\le m_4^{(p)}\right),$$

$$x_{0,j}^{(p,1)}=x_*^{(p)}\left(\psi_j^{(p,1)}\right),\ \ y_{0,j}^{(p,1)}=0\ \left(0\le j\le n_1^{(p)}\right),$$

$$x_{0,j}^{(p,2)}=x_*^{(p)}\left(\psi_j^{(p,2)}\right),\ \ y_{0,j}^{(p,2)}=0\ \left(0\le j\le n_2^{(p)}\right),$$

$$x_{m_3^{(p)},j}^{(p,3)}=x^{*(p)}\left(\psi_j^{(p,3)}\right),\ \ y_{m_3^{(p)},j}^{(p,3)}=0\ \left(0\le j\le n_3^{(p)}\right),$$

$$x_{m_4^{(p)},j}^{(p,4)}=x^{*(p)}\left(\psi_j^{(p,4)}\right),\ \ y_{m_4^{(p)},j}^{(p,4)}=0\ \left(0\le j\le n_4^{(p)}\right),$$

$$-a/2\le x_{m_1^{(p)},j}^{(p,1)}\le x_{\underline{Q}}^{(p)},\ \ y_{m_1^{(p)},j}^{(p,1)}=b\ \left(0\le j\le n_{B^1}^{(p)}\right),$$

$$x_{m_1^{(p)},j}^{(p,1)}=-a/2,\ \ 0\le y_{m_1^{(p)},j}^{(p,1)}\le b\ \left(n_{B^1}^{(p)}+1\le j\le n_1^{(p)}\right),$$

$$x_{\underline{Q}}^{(p)}\le x_{0,j}^{(p,4)}\le a/2,\ \ y_{0,j}^{(p,4)}=b\ \left(0\le j\le n_{C^1}^{(p)}\right),$$

$$x_{0,j}^{(p,4)}=a/2,\ \ 0\le y_{0,j}^{(p,4)}\le b\ \left(n_{C^1}^{(p)}+1\le j\le n_4^{(p)}\right); \quad (17)$$

$$x_{i,n_1^{(p)}}^{(p,1)}=x_{i,n_1^{(p)}-1}^{(p,1)},\ \ i=\overline{1,m_1^{(p)}-1},\ \ x_{i,0}^{(p,2)}=x_{i,1}^{(p,2)},$$

$$i=\overline{1,m_2^{(p)}},\ \ x_{i,0}^{(p,3)}=x_{i,1}^{(p,3)},\ \ i=\overline{0,m_3^{(p)}-1},$$

$$x_{i,n_4^{(p)}}^{(p,4)}=x_{i,n_4^{(p)}-1}^{(p,4)},\ \ i=\overline{1,m_4^{(p)}-1},$$

$$x_{m_1^{(p)},0}^{(p,1)}=x_{m_2^{(p)},n_2^{(p)}}^{(p,2)}=x_{0,n_3^{(p)}}^{(p,3)}=x_{0,0}^{(p,4)}=x_{0,n_3^{(p)}-1}^{(p,3)},$$

$$x_{0,j}^{(p,1)}=x_{1,j}^{(p,1)},\ \ j=\overline{0,n_1^{(p)}-1},\ \ x_{0,j}^{(p,2)}=x_{1,j}^{(p,2)},\ \ j=\overline{1,n_2^{(p)}},$$

$$x_{m_3^{(p)},j}^{(p,3)}=x_{m_3^{(p)}-1,j}^{(p,3)},\ \ j=\overline{1,n_3^{(p)}},\ \ x_{m_4^{(p)},j}^{(p,4)}=x_{m_4^{(p)}-1,j}^{(p,4)},$$

$$j=\overline{0,n_4^{(p)}-1},\ \ x_{m_1^{(p)},j}^{(p,1)}=x_{m_1^{(p)}-1,j}^{(p,1)},\ \ j=\overline{1,n_{B^1}^{(p)}},$$

$$y_{m_1^{(p)},j}^{(p,1)}=y_{m_1^{(p)}-1,j}^{(p,1)},\ \ j=\overline{n_{B^1}^{(p)},n_1^{(p)}-1},\ \ x_{0,j}^{(p,4)}=x_{1,j}^{(p,4)},$$

$$j=\overline{1,n_{C^1}^{(p)}},\ \ y_{0,j}^{(p,4)}=y_{1,j}^{(p,4)},\ \ j=\overline{n_{C^1}^{(p)},n_4^{(p)}-1}; \quad (18)$$

$$\Phi(\sigma)=\sum_{p,\xi=1}^{df}\sum_{i,j}^{\tilde{p},\tilde{A}}\left(\begin{array}{l}\sigma\left(\begin{array}{l}x_{i,j}^{(p,\xi)},y_{i,j}^{(p,\xi)},\chi,\alpha_1,\varepsilon_1,\\ x_1,y_1,...,\alpha_s,\varepsilon_s,x_s,y_s\end{array}\right)-\\ -\dfrac{d\left(z_{i-1,j-1}^{(p,\xi,J)},z_{i+1,j-1}^{(p,\xi,J)}\right)+d\left(z_{i-1,j+1}^{(p,\xi,J)},z_{i+1,j+1}^{(p,\xi,J)}\right)}{d\left(z_{i-1,j-1}^{(p,\xi,J)},z_{i-1,j+1}^{(p,\xi,J)}\right)+d\left(z_{i+1,j-1}^{(p,\xi,J)},z_{i+1,j+1}^{(p,\xi,J)}\right)}\times\\ \times\dfrac{1}{\tilde{\gamma}^{(p,\xi)}}\end{array}\right)^2. \quad (19)$$

Here $\gamma^{(p,\xi)}$ are quasiconformal invariants [8] for domains $G_{\omega}^{\gamma(p,\xi)}$;

$\left(x_{m_1^{(p)},n_{B^1}^{(p)}}^{(p,1)},y_{m_1^{(p)},n_{B^1}^{(p)}}^{(p,1)}\right)$ and $\left(x_{0,n_{C^1}^{(p)}}^{(p,4)},y_{0,n_{C^1}^{(p)}}^{(p,4)}\right)$

are nodes with discharges

$$\left[Q_{B^1}^{(p)} / \Delta\psi^{(p,1)}\right]\Delta\psi^{(p,1)} \text{ and } \left[Q_{C^1}^{(p)} / \Delta\psi^{(p,4)}\right]\Delta\psi^{(p,4)}$$

through sections $\overline{O}_pB^0$ and $\overline{O}_pC^0$, respectively; indices and values of quasiconformal invariants of formulas (16) and (19) are determined in accordance with the Table 1, and expressions (19) are taken into account only at nodes with a relatively large value of the geometric factor;

$$d(z_1,z_2)=\sqrt{(x_2-x_1)^2+(y_2-y_1)^2};$$

$$x_{i,j}^{(p,\xi)}=x^{(p,\xi)}\left(\varphi_i^{(p,\xi)},\psi_j^{(p,\xi)}\right),$$

$$y_{i,j}^{(p,\xi)}=y^{(p,\xi)}\left(\varphi_i^{(p,\xi)},\psi_j^{(p,\xi)}\right),$$

$$\sigma_{i,j}^{\gamma(p,\xi)}=\sigma\left(x_{i,j}^{(p,\xi)},y_{i,j}^{(p,\xi)}\right),\ \left(x_{i,j}^{(p,\xi)},y_{i,j}^{(p,\xi)}\right)\in G_z^{(p,\xi)},$$

$$p=\overline{1,\tilde{p}},\ \ \xi=\overline{1,4};$$

$$x_{i,-1}^{(p,1)}=x_{i,n_2^{(p)}-1}^{(p,2)},\ \ y_{i,-1}^{(p,1)}=y_{i,n_2^{(p)}-1}^{(p,2)},\ \ x_{i,n_2^{(p)}+1}^{(p,2)}=x_{i,1}^{(p,1)},$$

$$y_{i,n_2^{(p)}+1}^{(p,2)}=y_{i,1}^{(p,1)},\ \ x_{-1,j}^{(p,3)}=x_{m_2^{(p)}-1,j}^{(p,2)},\ \ y_{-1,j}^{(p,3)}=y_{m_2^{(p)}-1,j}^{(p,2)},$$

$$x_{m_2^{(p)}+1,j}^{(p,2)}=x_{1,j}^{(p,3)},\ \ y_{m_2^{(p)}+1,j}^{(p,2)}=y_{1,j}^{(p,3)},\ \ x_{i,-1}^{(p,4)}=x_{i,n_3^{(p)}-1}^{(p,3)},$$

$$y_{i,-1}^{(p,4)}=y_{i,n_3^{(p)}-1}^{(p,3)},\ \ x_{i,n_3^{(p)}+1}^{(p,3)}=x_{i,1}^{(p,4)},\ \ y_{i,n_3^{(p)}+1}^{(p,3)}=y_{i,1}^{(p,4)}.$$

Table 1

Dependencies between indices and values of quasiconformal invariants of formulas (16) and (19)

ξ	i	j	$\tilde{\gamma}^{(p,\xi)}$
1, 2, 3, 4	$\overline{1,m_\xi^{(p)}-1}$	$\overline{1,n_\xi^{(p)}-1}$	$\gamma^{(p,\xi)}$
1, 4	$\overline{1,m_\xi^{(p)}-1}$	0	$\sqrt{\gamma^{(p,\xi)}\gamma^{(p,(\xi+5)/3)}}$
2	$m_2^{(p)}$		

It is worth noting [8] that the difference formula (16) was constructed using a «cross» type scheme and is used for a relatively quick refinement of the coordinates of the internal nodes of electrodynamic networks. Expressions (17) and (18) are orthogonality conditions and boundary conditions, respectively; the first of them are formed using left and right first order difference schemes. Minimizing functional (19) is intended for direct identification of the CC and is constructed from considerations of quasiconformal similarities in small curvilinear quadrangles of two similarities.

6. Algorithm for the numerical solution of the difference problem (16)–(19)

It consists in the alternate parameterization of quasiconformal invariants, internal and part of the limit nodes of network domains and CC, using the ideas of the block iteration method [8–10]. First of all, let's set the following data:

1) auxiliary parameters q_1 and q_2, accuracy parameter ε, number of bursts s, number of injection $\tilde{p}$, approximation numbers $l=0$ and $r=0$ of the sought functions and parameters;

2) quasipotentials $\varphi_*^{(p)}, \varphi_0^{(p)}, \varphi^{*(p)}$, and discharges $Q_{12}^{(p)}$ and $Q_{34}^{(p)}$ in the corresponding sections A_pB_p and C_pD_p;

3) initial approximations of the CC parameters $\chi^{(l)}$, $\alpha_k^{(l)}$, $\varepsilon_k^{(l)}$, $x_k^{(l)}$, $y_k^{(l)}$ $(k=1,...,s)$;

4) the number of nodes for dividing networks in Fig. 1,

$$m_1^{(p)},\ \ m_2^{(p)}=m_1^{(p)},$$

$$m_3^{(p)}=\left[m_1^{(p)}\frac{\varphi^{*(p)}-\varphi_0^{(p)}}{\varphi_0^{(p)}-\varphi_*^{(p)}}+0.5\right],$$

$$m_4^{(p)}=m_3^{(p)},$$

$$n_{12}^{(p)}=\left[m_1^{(p)}\frac{Q_{12}^{(p)}}{\varphi_0^{(p)}-\varphi_*^{(p)}}+0.5\right],$$

$$n_{34}^{(p)}=\left[m_4^{(p)}\frac{Q_{34}^{(p)}}{\varphi^{*(p)}-\varphi_0^{(p)}}+0.5\right],$$

$$n_\xi^{(p,l)}=\left[0.5\min(n_{12}^{(p)},n_{34}^{(p)})+0.5\right]$$

$$(\xi=2,3),\ n_1^{(p,l)}=n_{12}^{(p)}-n_2^{(p,l)},\ \ n_4^{(p,l)}=n_{34}^{(p)}-n_3^{(p,l)},$$

$$n_{B^1}^{(p,l)}\ \ (n_{B^1}^{(p,l)}<n_1^{(p,l)}),\ \ n_{C^1}^{(p,l)}\ \ (n_{C^1}^{(p,l)}<n_4^{(p,l)});$$

5) parameters for specifying key points on the boundaries $x_A^{(p)}, x_B^{(p)}, x_C^{(p)}, x_D^{(p)}$;

6) width a and height b of the investigated area;

7) coordinates of boundary (on sections $B^0B^1C^1C^0$):

$$x_{i,n_1^{(p)}}^{(p,1)},\ y_{i,n_1^{(p)}}^{(p,1)}\ \left(i=\overline{0,m_1^{(p)}}\right),$$

$$x_{i,0}^{(p,2)},\ y_{i,0}^{(p,2)}\ \left(i=\overline{0,m_2^{(p)}}\right),\ \ x_{i,0}^{(p,3)},\ y_{i,0}^{(p,3)}\ \left(i=\overline{0,m_3^{(p)}}\right),$$

$$x_{i,n_4^{(p)}}^{(p,4)},\ y_{i,n_4^{(p)}}^{(p,4)}\ \left(i=\overline{0,m_4^{(p)}}\right),\ \ x_{0,j}^{(p,1)},\ y_{0,j}^{(p,1)}\ \left(j=\overline{0,n_1^{(p)}}\right),$$

$$x_{0,j}^{(p,2)},\ y_{0,j}^{(p,2)}\ \left(j=\overline{0,n_2^{(p)}}\right),$$

$$x_{m_3^{(p)},j}^{(p,3)},\ y_{m_3^{(p)},j}^{(p,3)}\ \left(j=\overline{0,n_3^{(p)}}\right),\ \ x_{m_4^{(p)},j}^{(p,4)},\ y_{m_4^{(p)},j}^{(p,4)}\ \left(j=\overline{0,n_4^{(p)}}\right)$$

and internal $x_{i,j}^{(p,\xi,l)}$, $y_{i,j}^{(p,\xi,l)}$

$$\left(i=\overline{1,m_\xi^{(p)}-1},\ j=\overline{0,n_\xi^{(p,l)}-1},\ \xi=1,4\right),$$

$$x_{i,j}^{(p,\xi,l)},\ \ y_{i,j}^{(p,\xi,l)}\ \ \left(i=\overline{1,m_\xi^{(p)}-1},\ j=\overline{1,n_\xi^{(p,l)}},\ \xi=2,3\right),$$

$$x_{0,j}^{(p,3,l)}=x_{m_2^{(p)},j}^{(p,2,l)},\ \ y_{0,j}^{(p,3,l)}=y_{m_2^{(p)},j}^{(p,2,l)}\ \ \left(j=\overline{1,n_2^{(p,l)}-1}\right)$$

nodes;

8) quasipotentials $\overline{\varphi}_{\overline{i}^{(p)}}^{(p)}$, $\overline{\overline{\varphi}}_{\overline{\overline{i}}^{(p)}}^{(p)}$, $\underline{\varphi}_{\underline{i}^{(p)}}^{(p)}$ local current densities $\Psi_{*j_*^{(p)}}^{(p)}$, $\Psi_{j^{*(p)}}^{*(p)}$ (and consequently, $\psi_*^{(p)}(M)$, $\psi^{*(p)}(M)$) in the points

$$\left(\overline{x}_{\overline{i}^{(p)}}^{(p)},\overline{y}_{\overline{i}^{(p)}}^{(p)}\right),\ \ \left(\overline{\overline{x}}_{\overline{\overline{i}}^{(p)}}^{(p)},\overline{\overline{y}}_{\overline{\overline{i}}^{(p)}}^{(p)}\right),$$

$$\left(\underline{x}_{\underline{i}^{(p)}}^{(p)},\underline{y}_{\underline{i}^{(p)}}^{(p)}\right),\ \ \left(x_{*j_*^{(p)}}^{(p)},y_{*j_*^{(p)}}^{(p)}\right),$$

$$\left(x_{j^{*(p)}}^{*(p)},y_{j^{*(p)}}^{*(p)}\right),$$

on the basis of which the functions is built

$$x=\bar{x}^{(p)}(\varphi),\quad x=\underline{x}^{(p)}(\varphi),\quad x=\bar{\bar{x}}^{(p)}(\varphi),$$

$$x=x_*^{(p)}(\psi),\quad x=x^{*(p)}(\psi)$$

by interpolation.

Let's calculate

$$\Delta\varphi^{(p,\xi)}=\left(\varphi_0^{(p)}-\varphi_*^{(p)}\right)/m_\xi^{(p)}\ \ (\xi=1,2),$$

$$\Delta\varphi^{(p,\xi)}=\left(\varphi^{*(p)}-\varphi_0^{(p)}\right)/m_\xi^{(p)}\ \ (\xi=3,4),$$

coordinates of boundary nodes

$$x_{m_1^{(p)},j}^{(p,1,l)},\quad y_{m_1^{(p)},j}^{(p,1,l)}\ \left(j=\overline{0,n_1^{(p,l)}-1}\right),$$

$$x_{0,j}^{(p,4,l)},\quad y_{0,j}^{(p,4,l)}\ \left(j=\overline{0,n_4^{(p,l)}-1}\right),$$

$$x_{m_2^{(p)},n_2^{(p,l)}}^{(p,2,l)}=x_{0,n_3^{(p,l)}}^{(p,3,l)}=x_{m_1^{(p)},0}^{(p,1,l)},\quad y_{m_2^{(p)},n_2^{(p,l)}}^{(p,2,l)}=y_{0,n_3^{(p,l)}}^{(p,3,l)}=y_{m_1^{(p)},0}^{(p,1,l)}\quad(20)$$

on the sections $B_pA_pD_pC_p$ by formula (17) and quasiconformal invariants

$$\gamma^{(p,\xi,l)}=\frac{4}{m_\xi^{(p)}n_\xi^{(p,l)}}\times$$

$$\times\sum_{i,j=0}^{m_\xi^{(p)}-1,n_\xi^{(p,l)}-1}\frac{d\left(z_{i,j}^{(p,\xi,l)},z_{i+1,j}^{(p,\xi,l)}\right)+d\left(z_{i,j+1}^{(p,\xi,l)},z_{i+1,j+1}^{(p,\xi,l)}\right)}{\sigma_{i,j}^{(p,\xi,l)}+\sigma_{i+1,j}^{(p,\xi,l)}+\sigma_{i,j+1}^{(p,\xi,l)}+\sigma_{i+1,j+1}^{(p,\xi,l)}}\Bigg/\begin{pmatrix}d\left(z_{i,j}^{(p,\xi,l)},z_{i,j+1}^{(p,\xi,l)}\right)+\\+d\left(z_{i+1,j}^{(p,\xi,l)},z_{i+1,j+1}^{(p,\xi,l)}\right)\end{pmatrix},\ \xi=\overline{1,4}.\quad(21)$$

For $p=\overline{1,\tilde{p}}$ successively iteratively refine the quasiconformal invariants $\gamma^{(p,\xi,l)}$, all internal and some of the limit nodes (20) according to formulas (21), (16) and (17), (18), respectively, with a simultaneous increase in the parameter l. At the same time, it should not be allowed that $n_{B^1}^{(p,l)}<4$ and $n_{C^1}^{(p,l)}<4$; the equations of systems (17), (18) must be combined in such a way that the distances between the boundary and limiting nodes become as small as possible. Further, every q_1 iterations, let's check simultaneously

$$\frac{\gamma^{(p,2,l)}m_2^{(p)}+\gamma^{(p,3,l)}m_3^{(p)}}{m_2^{(p)}+m_3^{(p)}}<\frac{\gamma^{(p,1,l)}+\gamma^{(p,4,l)}}{2},$$

$$n_1^{(p,l)}>10,\ n_4^{(p,l)}>10.$$

In the positive case, it is possible to decrease $n_1^{(p,l)}$, $n_4^{(p,l)}$ and increase the case $n_2^{(p,l)}$, $n_3^{(p,l)}$, if, on the contrary

$$\frac{\gamma^{(p,2,l)}m_2^{(p)}+\gamma^{(p,3,l)}m_3^{(p)}}{m_2^{(p)}+m_3^{(p)}}>\frac{\gamma^{(p,1,l)}+\gamma^{(p,4,l)}}{2},\quad n_2^{(p,l)}>10,$$

then decrease $n_2^{(p,l)}$, $n_3^{(p,l)}$ and increase $n_1^{(p,l)}$, $n_4^{(p,l)}$. Moreover, every q_2 iterations, let's check the grid nodes are sufficiently stabilized, for example, using formulas [8]. In the positive case, let's increase r and refine the CC parameters $\chi^{(r)}$, $\alpha_k^{(r)}$, $\varepsilon_k^{(r)}$, $x_k^{(r)}$, $y_k^{(r)}$ ($k=1,...,s$) using one of the global optimization methods, for example, [11] according to formula (19). If $|\Phi^{(r)}-\Phi^{(r-1)}|<\varepsilon$ (let's fictitiously set $\Phi^{(0)}=0$), then let's complete the iterative process, display the reconstructed image and, if necessary, electrodynamic grids, domains of the complex quasipotential, fields of current densities, discharges $Q_\xi^{(p)}=\Delta\varphi^{(p,\xi)}/\Delta\gamma^{(p,\xi,l)}$ ($\xi=\overline{1,4}$), and the like. Otherwise, let's start the iterative process again.

7. Results of numerical calculations of CC parameters by means of ERT inside a fragment of a soil massif

Numerical calculations were carried out on the basis of data obtained using a full-range gradient array [2, 4]. In this case, the solution of the difference problem (1), (16)–(18) is proposed to be performed not in a single domain in Fig. 1, *a*, and in sufficiently large $\tilde{p}_h$ subdomains with longitudinal $a_p=\underline{x_C^{(p)}}-x_B^{(p)}+180$ and transverse $b_p=0.5a_p$ dimensions ($p=\overline{1,\tilde{p}}$). With such a division into subproblems, on the one hand, there are sufficiently small values of the geometric factor at the boundaries, and on the other hand, savings in computer time are provided. Here $a=a_p$, $b=b_p\left(B^0=B_p^0,C^0=C_p^0,B^1=B_p^1,C^1=C_p^1\right)$.

Fig. 2 shows examples of computational grids for the 1st and 200th injection. The procedure itself for specifying network nodes is carried out not for $\tilde{p}$ situational cases of application of quasipotentials with a fixed CC, but for $\tilde{p}$ different variants of the CC distribution with «block» fixed sections of application of quasipotentials.

In this case, in order to speed up the calculations, it is worth choosing the initial approximations of the coordinates of the nodes of the next injection as calculated from the preliminary injection. For the convenience of calculations, let's also introduce the parameters $\tilde{p}_w$ and $\tilde{p}_h$ [2] to designate the total number of application areas of quasipotentials and different application distances, respectively.

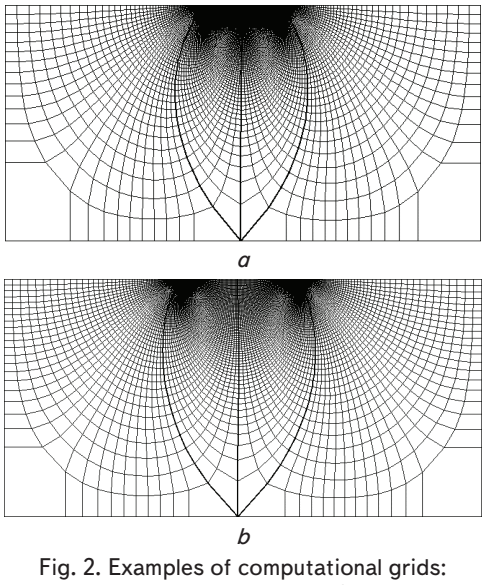

a

b

Fig. 2. Examples of computational grids: for *a* – 1st injection; *b* – 200th injection

Experimental data on the values of the functions of the quasipotential and local current densities along the sections $B_p^0A_pB_pD_pC_pC_p^0$, for the given CC parameters χ, α_k, ε_k, x_k, y_k ($k=1,...,s$) and potentials $\varphi_*^{(p)}$, $\varphi_0^{(p)}$, $\varphi^{*(p)}$, were obtained using the program for simulating a physical experiment developed earlier. At given

$q_1=50$, $q_2=200$, $s=1$,

$\tilde{p}_h=2$, $\tilde{p}_w=61$, $\tilde{p}=(\tilde{p}_w-\tilde{p}_h+1)$,

$$m_1^{(p)} = 80, \quad n_{B^1}^{(p,l)} = n_{C^1}^{(p,l)} = 5,$$

$$0.1 \le \chi \le 2, \ -2 \le \alpha_k \le 2, \ 1 \le \varepsilon_k \le 10{,}000,$$

$$-0.25a_p \le x_k \le 0.25a_p, \ 0 \le y_k \le 0.5b_p,$$

$$\chi^{(l)} = 1, \quad \alpha_k^{(l)} = 0, \quad \varepsilon_k^{(l)} = 1,$$

$$x_k^{(l)} = 0, \quad y_k^{(l)} = 0 \quad \left(l = 0, k = \overline{1,s}\right),$$

$$x_A^{(p)} = -5(p_h + 1),$$

at

$$\begin{pmatrix} \tilde{p}_w + p_h - \\ 2\tilde{p}_h \end{pmatrix}(p_h \quad 1) < p \le \begin{pmatrix} \tilde{p}_w + p_h - \\ 2\tilde{p}_h + 1 \end{pmatrix} p_h,$$

$$x_D^{(p)} = -x_A^{(p)}, \quad x_B^{(p)} = x_A^{(p)} - 10, \quad x_C^{(p)} = x_D^{(p)} + 10,$$

$$\varphi_*^{(p)} = -2, \quad \varphi_0^{(p)} = 0, \quad \varphi^{*(p)} = 2 \quad \left(p = \overline{1,\tilde{p}}, p_h = \overline{1,\tilde{p}_h}\right)$$

and the known standard Fig. 3, *a* and the computational process turned out to be convergent, and the solution (Fig. 3, *b*) «within reasonable limits» corresponds to the expected one. Such results were achieved even if the requirement for the depth of research was not met, which, according to [2], should not exceed 1/3–1/6 of the maximum distance between the A_pB_p and C_pD_p domains.

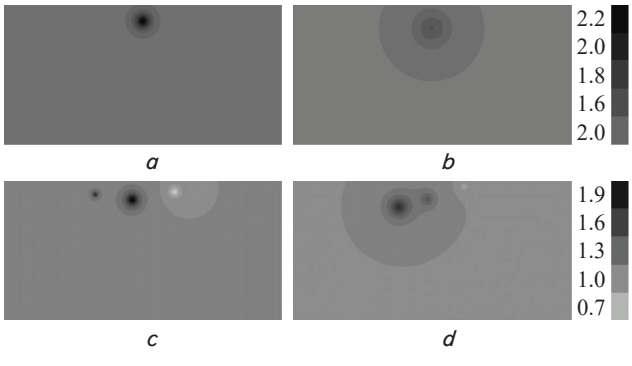

Fig. 3. Tomographic image of the distribution of CC values in grayscale: *a* – standard with one burst ($\chi = 1.3$, $\alpha_0 = 1$, $\varepsilon_0 = 120$, $x_0 = 0$, $y_0 = 30$); *b* – reconstructed image; *c* – standard with three bursts ($\chi = 1$, $\alpha_0 = 0.7$, $\varepsilon_0 = 20$, $x_0 = -90$, $y_0 = 25$, $\alpha_1 = 1$, $\varepsilon_1 = 100$, $x_1 = -20$, $y_1 = 35$, $\alpha_2 = -0.55$, $\varepsilon_2 = 50$, $x_2 = 60$, $y_2 = 20$); *d* – corresponding reconstructed image

Complicating the structure of the environment by setting $s=3$ bursts and increasing the amount of input data using the parameter $\tilde{p}_h=4$, the image in Fig. 3, *d* with reference Fig. 3, *c*.

8. Discussion of the results of an approximate solution to the problem of reconstructing the image of a fragment of a soil massif by ERT means

As is known [1], when solving problems by ERT means, there is no general mechanism for comparing the quality of the obtained images with the reference ones. Since most often ERT is used only to determine the coordinates of inhomogeneities in the domain [1, 2, 12], then, similarly to [9], as the main criterion, let's take the residuals of the distances between the «peaks» of the CC values.

In Fig. 3, *b* for the calculated parameters

$$\hat{\chi} = 1.271533, \quad \hat{\alpha}_0 = 0.3321661, \quad \hat{\varepsilon}_0 = 919.6152,$$

$$\hat{x}_0 = -1.254098, \quad \hat{y}_0 = 43.75537,$$

the discrepancy of the coordinates of the bursts is 13.81242. With only $\tilde{p}_h=2$, this result can be explained by a small number of the sought parameters. At the same time, functional (19) takes the value 58249, which on average corresponds to an error of 0.018 per node, however, obviously, it reaches significantly larger values in some areas.

In Fig. 3, *d* with the calculated parameters

$$\hat{\chi} = 0.9853642, \quad \hat{\alpha}_0 = 0.3160008, \quad \hat{\varepsilon}_0 = 152.4604,$$

$$\hat{x}_0 = -8.698875, \quad \hat{y}_0 = 33.48841, \quad \hat{\alpha}_1 = -0.2597447,$$

$$\hat{\varepsilon}_1 = 27.3199, \quad \hat{x}_1 = 59.79078, \quad \hat{y}_1 = 10.39442,$$

$$\hat{\alpha}_2 = 0.6426869, \quad \hat{\varepsilon}_2 = 243.1526, \quad \hat{x}_2 = -62.94914,$$

$$\hat{y}_2 = 48.82635$$

discrepancy of the coordinates of the «peaks» of the CC values are as follows: 36.71644, 11.40177, 9.60786. In this case, functional (19) takes on the value 194031, which on average corresponds to an error of 0.045 per node.

In both cases under consideration, similar dynamics of distributions of CC values are observed in comparison with the reference ones. Namely: as expected [10], the calculated images are blurred, that is, lower CC values were obtained at the centers of the bursts at their large scales. In this case, the coordinates of the reconstructed «peaks» along the *y*-axis are lower than on the reference. These facts are explained, on the one hand, by the properties of functionals of the form (15), which minimize the square of the error at a number of nodes simultaneously, and, on the other hand, by the errors of the method of quasiconformal mappings. The level of the latter can be somewhat reduced in one of the following ways:

– increase in the number of sections for the simultaneous application of quasipotentials, which, however, can lead to too much condensation of the vicinity of a significant violation of quasiconformality; this can be solved by «replacing» the smoothness at the corner points with orthogonality;

– use of precise data types in order to reduce the rounding error accumulated in the computational process, which, on the other hand, negatively affects the speed of calculations;

– use of accurate meshing schemes, on the other hand, will slow down computations;

– prevention of large areas of violation of quasiconformity around points B_p^1, C_p^1 by changing the shape of equipotential lines $B_p^0B_p^1C_p^1C_p^0$ to smoother;

– by setting greater accuracy of the completion of the calculation process: both at the stage of simulating a physical experiment, and in the process of identifying the CC.

The problems that arise due to the form of functional (15), like [1, 3], can be partially solved by a significant change in its form or regularization.

It should be noted that this study concerns isotropic media with available bursts of CC values. But similarly to [9], the corresponding studies can be easily extended to other media, including anisotropic ones. However, in the latter case, it is necessary to have additional information about the structure of the conductivity tensor [1, 6, 9].

The carried out research is also easy to extend to the case of curved soil surfaces [2, 12]. However, it is important here that there are conditions for fixing the electrodes in sufficiently large areas; otherwise, make a decision on the use of a different charge injection scheme [2, 4, 5]. In particular, the permissible depth of research substantially depends on the latter [2, 5].

The calculated image is not always easy to interpret correctly, primarily due to the similar electrical characteristics of a number of components of the soil massif. For example [2], lignite, depending on its state, has the same CC values as fresh water.

The study, similar to [2], does not concern the reconstruction of the image of too deep soil layers. Problems also remain in identifying the parameters of highly contrasting media.

In the future: transfer of the developed algorithm to space [2], anisotropy [1, 6, 9] and cases of piecewise homogeneous media [2] using the conditions of non-ideal contact [13]. In addition, it is important to develop mechanisms for bringing various additional conditions to the studied environment, in particular, discrete data from deep soil layers [2, 4, 6]. It is also advisable to develop an approach developed for the cases of reconstruction of the image of the middle verdure space [2, 4, 6]. An important issue is the parallelization of computations like [9], taking into account the large volumes of computations.

9. Conclusions

1. The method developed in [10] for reconstructing images of solid objects with known additional conditions along the entire boundary is transferred in the case of identifying the parameters of the structures of fragments of soil massifs with uneven setting of additional boundary conditions. At the same time, the reconstruction of the image occurs only in the subdomain in which the value of the geometric factor is relatively large. The peculiarity and advantage of the proposed approach is not only to avoid the use of the Dirac delta functions, that is, the «pointness» of the electrode application areas, but also the use of qualitatively new data at the potential application areas. In addition, it is assumed, for each of the corresponding injection, the presence on the boundary of the domain of only equipotential lines, with given functions of local current densities, and streamlines, with known distributions of the quasipotential on them.

2. An algorithm for reconstructing the image of a fragment of a soil massif by means of electrical resistivity tomography with an uneven distribution of data along the border has been developed. It provides for a sequential parameterization of the values of quasiconformal invariants, internal and part of the limit nodes of network domains and the conductivity coefficient, using the ideas of the block iteration method. In order to speed up the computations, a modification of the above algorithm is also proposed.

3. The prospect of further practical implementation of the proposed method follows from its ability to give an approximate result at a relatively low cost. In particular, although with an increase in the distance from the contact electrodes the maximum quality of reconstruction rapidly decreases, nevertheless, it is possible to reduce the level of error by minimizing the functional. This will allow obtaining more accurate solutions, first of all, in the subdomain with a sufficiently large value of the geometric factor. This effect can be achieved by reducing the size of the quasiconformity violation areas, using more accurate data types and difference schemes in computer calculations.

References

1. Holder, D. (Ed.) (2004). Electrical Impedance Tomography. Methods, History and Applications. CRC Press, 456. doi: https://doi.org/10.1201/9781420034462
2. Loke, M. H. (2020). Tutorial: 2-D and 3-D electrical imaging surveys. Available at: https://www.geotomosoft.com/coursenotes.zip
3. Pekker, Ya. S., Brazovskiy, K. S., Usov, V. Yu., Plotnikov, M. P., Umanskiy, O. S. (2004). Elektroimpedansnaya tomografiya. Tomsk: NTL, 192.
4. Kanli, A. I. (Ed.) (2019). Applied Geophysics with Case Studies on Environmental, Exploration and Engineering Geophysics. London: IntechOpen. doi: https://doi.org/10.5772/intechopen.78490
5. Dahlin, T., Zhou, B. (2005). Multiple-gradient array measurements for multichannel 2D resistivity imaging. Near Surface Geophysics, 4 (2), 113–123. doi: https://doi.org/10.3997/1873-0604.2005037
6. Herwanger, J. V., Pain, C. C., Binley, A., de Oliveira, C. R. E., Worthington, M. H. (2004). Anisotropic resistivity tomography. Geophysical Journal International, 158 (2), 409–425. doi: https://doi.org/10.1111/j.1365-246x.2004.02314.x
7. Pessel, M., Gibert, D. (2003). Multiscale electrical impedance tomography. Journal of Geophysical Research: Solid Earth, 108 (B1). doi: https://doi.org/10.1029/2001jb000233
8. Bomba, A. Ya., Kashtan, S. S., Pryhornytskyi, D. O., Yaroshchak, S. V. (2013). Metody kompleksnoho analizu. Rivne: Natsionalnyi universytet vodnoho hospodarstva ta pyrodokorystuvannia, 430.
9. Bomba, A. Y., Kuzlo, M. T., Michuta, O. R., Boichura, M. V. (2019). On a method of image reconstruction of anisotropic media using applied quasipotential tomographic data. Mathematical Modeling and Computing, 6 (2), 211–219. doi: https://doi.org/10.23939/mmc2019.02.211
10. Bomba, A., Boichura, M. (2017). On a numerical quasiconformal mapping method for the medium parameters identification using applied quasipotential tomography. Mathematical Modeling and Computing, 4 (1), 10–20. doi: https://doi.org/10.23939/mmc2017.01.010
11. Aguiar e Oliveira Junior, H., Ingber, L., Petraglia, A., Rembold Petraglia, M., Augusta Soares Machado, M. (2012). Stochastic Global Optimization and Its Applications with Fuzzy Adaptive Simulated Annealing. Heidelberg: Springer-Verlag. doi: https://doi.org/10.1007/978-3-642-27479-4
12. Rymarczyk, T., Adamkiewicz, P. (2017). Monitoring damage and dampness in flood embankment by electrical impedance tomography. Informatics Control Measurement in Economy and Environment Protection, 7 (1), 59–62. doi: https://doi.org/10.5604/01.3001.0010.4584
13. Ulyanchuk-Martyniuk, O., Michuta, O., Ivanchuk, N. (2020). Biocolmation and the finite element modeling of its influence on changes in the head drop in a geobarrier. Eastern-European Journal of Enterprise Technologies, 4 (10 (106)), 18–26. doi: https://doi.org/10.15587/1729-4061.2020.210044